A&A 466, 1205–1210 (2007)
DOI: 10.1051/0004-6361:20066236

Astronomy & Astrophysics

The ISOPHOT 170 μm Serendipity Survey

IV. The far-infrared sky atlas⋆,⋆⋆

M. Stickel, O. Krause, U. Klaas, and D. Lemke

Max-Planck-Institut für Astronomie, Königstuhl 17, 69117 Heidelberg, Germany
e-mail: stickel@mpia.de

Received 11 August 2006 / Accepted 24 October 2006

ABSTRACT

Aims. To further increase the scientific utilization of the strip scanning measurements of the ISOPHOT Serendipity Survey (ISOSS), the slew data has been assembled to a sky atlas with ≈15% sky coverage in the hitherto unobserved far-infrared wavelength band around 170 μm.
Methods. The redundant information of the brightnesses at slew crossings has been used to globally rescale and homogenize the slew brightnesses, leading to significantly increased photometric accuracy and reproducibility as well as the homogeneity of the maps. The corrected slew data were mapped with a constant grid size of 22.″4 and are presented in 124 maps in galactic coordinates.
Results. The collection of image plates represents the ISOSS Sky Atlas, which will become available from major data archives. Exemplary scientific results are described, which show the scientific potential of the data set combined with far-infrared imaging data from previous and upcoming missions.

Key words. surveys – infrared: general – atlases – astronomical data bases: miscellaneous – methods: data analysis

1. Introduction

The Infrared Space Observatory ISO (Kessler et al. 1996; Kessler 1999) was the first space observatory to include a slew survey, dubbed the ISOPHOT Serendipity Survey (ISOSS), as an integral part of its mission. Scientific results were already obtained early into the mission (Bogun et al. 1996), and it successfully returned data throughout the whole ISO lifetime (Stickel et al. 1999). This is in contrast to other space observatories such as EINSTEIN and EXOSAT, where data taken during the slewing time between pointed observations have eventually been analyzed long after the end of the satellite's lifetime (Reynolds et al. 1999; Elvis et al. 1992).

The slewing of the telescope between individual pointings could have been quite long and thereby crossed a significant part of the sky, leading to an almost unbiased but incomplete survey beyond the IRAS 100 μm limit. The far-infrared wavelength of 170 μm had the prospect of delivering new photometric data not only for a large number of cold point or marginally extended sources but also for extended FIR emitting cold material distributed on large scales in the Galaxy.

The slew data streams can individually be analyzed and searched for compact sources, to obtain 170 μm photometry for a large variety of sources from galactic star forming regions to galaxies. A representative overview of these investigations can be found in Stickel et al. (2002, 2003). The analysis of the compact sources, with special emphasis on galaxies, as well as the resulting compact source database is described in Stickel et al. (1998a,b, 2000, 2004). As a second fundamentally different utilization of the ISOSS data, the slew streams have been assembled into two-dimensional sky maps, which allow the investigation of the FIR emitting material from the Galaxy on larger angular scales. In the following, the preparation of the ISOSS 170 μm Sky Atlas and the resulting set of sky images is described and applications and scientific results of the map data are demonstrated.

2. Data processing and image preparation

The ISOPHOT Serendipity Sky Survey Atlas is based on the slew measurements, which were carried out with the ISOPHOT C200 detector (Lemke et al. 1996), a 2×2 pixel array of stressed Ge:Ga (pixel size of 89.″4) and the C_160 broad band filter (reference wavelength 170 μm, equivalent width 89 μm), when the ISO satellite moved from one target to the next.

During the entire lifetime of ISO, which lasted 875 revolutions on a $24^{\rm h}$ orbit, more than 12 000 slews were executed. A total of about 550 h of observing time were gathered, with individual slews reaching lengths up to 150° and a total slew length exceeding 150 000° (Stickel et al. 2004). For longer slews with a duration of at least 75 s, the detector signals from the read-out ramps were converted to surface brightness by using a responsivity measurement of the on-board Fine Calibration Source, while for shorter slews the default calibration was used.

Slews were corrected for cosmic ray hits and pixel-to-pixel variations of the detector sensitivity (flat-fielding). Pointing information was refined at each sky position to correct for gyro

⋆ Based on observations with ISO, an ESA project with instruments funded by ESA Member States (especially the PI countries: France, Germany, The Netherlands and the United Kingdom) and with the participation of ISAS and NASA. Members of the Consortium on the ISOPHOT Serendipity Survey (CISS) are MPIA Heidelberg, ESAC Villafranca, AIP Potsdam, IPAC Pasadena, Imperial College London.

⋆⋆ Image files (FITS files) are available in electronic form at the CDS via anonymous ftp to cdsarc.u-strasbg.fr (130.79.128.5) or via
http://cdsweb.u-strasbg.fr/cgi-bin/qcat?J/A+A/466/1205
and the ISO Data Archive www.iso.vilspa.esa.es/

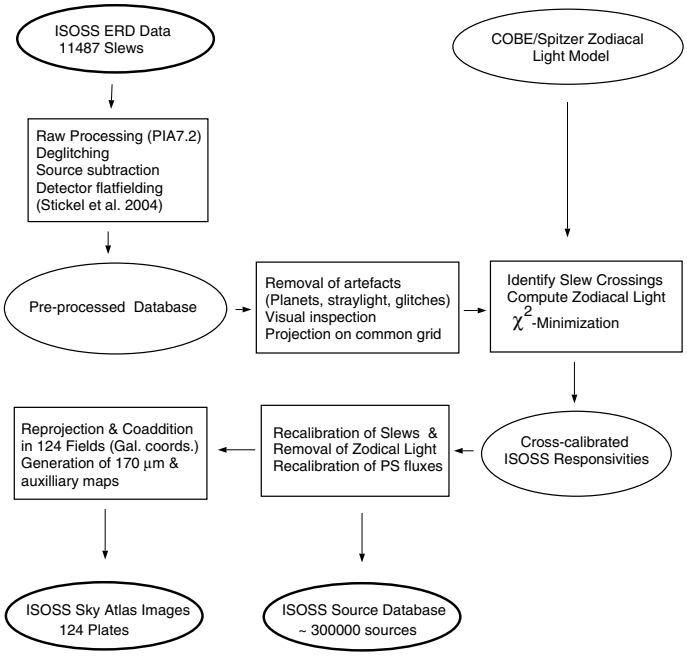

Fig. 1. Flow diagram summarizing the processing steps of the ISOSS slew data from the raw data streams to the final ISOSS Sky Atlas images and the ISOSS compact source database.

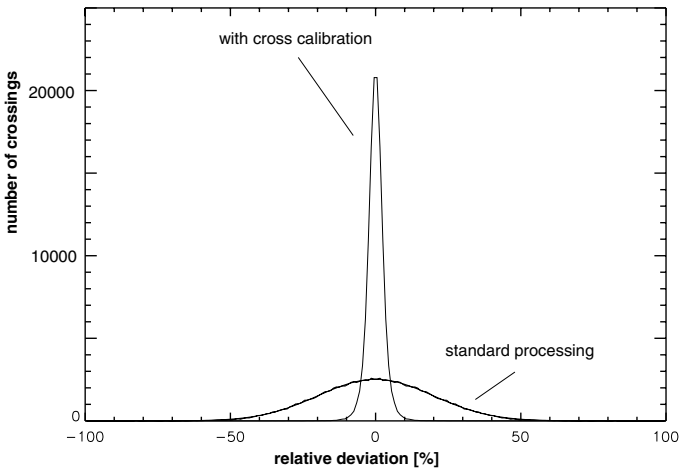

Fig. 2. The distribution of the relative differences of slew brightnesses at slew crossings. The width of the distribution after rescaling is an order of magnitude narrower than the original distribution obtained with the standard processing.

drifts between the two end points of slews. These steps eventually led to the identification and compilation of a database of compact galactic and extra-galactic sources. More details of the slew processing can be found elsewhere (Stickel et al. 2002, 2003, 2004). The atlas images are based on the products for the compact source analysis. The overall processing of the slew data with the final maps as the end product is summarized in the flow diagram in Fig. 1.

Early in the atlas preparation, it was recognized that individual slews crossing each other within a small region of the sky had not always the same levels, indicating differences in the individual calibrations. These were due to ionizing radiation inducing systematic variation of the detector responsivity along the orbit of ISO, which were not adequately reflected in the short measurement of the on-board Fine Calibration Source of ISOPHOT preceding the slews. Occassionally they came from strong hits of cosmic ray particles.

To avoid disturbing striping in the final maps, the individual slews were rescaled so as to minimize their mutual squared brightness differences. To avoid the influence of inaccuracies in the slew positions near compact sources, which would lead to strongly disagreeing brightness levels, the morphologically filtered (Sternberg 1986) and flat-fielded versions of the slew brightness time series has been used. The former low-pass filtering operation removes all compact sources up to an angular scale length with a full width at zero intensity of five times the FWHM (57″) of a gaussian approximation to the C200 170 μm beam profile. Conceptually, it is equivalent to rolling an Euclidian disk underneath the data stream and taking the upper hull given by the highest point of the rolling circle as the smooth background. A second secularly changing influence is the brightness of the zodiacal light, which was in turn subtracted by using the Spitzer zodiacal light model (Reach 2000) transformed to the ISOPHOT 170 μm filter. All crossings of two individual slews were identified, which resulted in a total of ≈270 000 crossings for nearly 10 000 slews.

The scaling factors $c_{j,k}$ for two slews at a particular crossing is then implicitly given by

$$c_j * I_j^\star - Z_j = c_k * I_k^\star - Z_k \tag{1}$$

where $I_{j,k}^\star$ is the morphologically filtered and flat-fielded 170 μm brightness and $Z_{j,k}$ the zodiacal light brightness at the slewing time. The scaling factors were then derived by minimizing the sum of the mutual deviations of all slew pairs globally over all crossings:

$$\chi^2 = \sum_{k>j} \left[\frac{c_j * I_j^\star - Z_j - c_k * I_k^\star + Z_k}{\sigma_{jk}} \right]^2 . \tag{2}$$

Equal weighting ($\sigma_{jk} = 1$) was chosen and the minimization problem was solved with the algorithm of Paige & Saunders (1982). This is an implementation of a conjugate-gradient iterative method with improved numerical properties for solving very large over- or underdetermined sparse least-squares problems. The comparison of the relative differences of the slew brightnesses at the crossings before and after the rescaling (Fig. 2) shows a significant decrease in the scatter of more than an order of magnitude, with about 90% of the data points having a relative flux deviation from the mean of less than 10%.

From the corrected slews, two-dimensional maps were produced with the Drizzle algorithm (Fruchter & Hook 2002). A pixel size of 22.″4 × 22.″4 was chosen to restore the full angular resolution of the detector at the crossings. The whole sky was covered with a mosaic of 124 maps with ≈20° × ≈20° size in gnomonic projection of galactic coordinates.

A comparsion of the resulting maps before and after slew rescaling is shown in Fig. 3, demonstrating the much better overall photometric quality of the final corrected maps and the capability to discern details at low surface brightness. Taking into account the uncertainty of the Spitzer Zodiacal Light model of 10% (Reach 2000) and transformation from 160 μm to the ISOSS 170 μm band, the accuracy of the final brightnesses in the ISOPHOT Sky Survey Atlas is ≲20%. This is better than the overall repeatability of the fluxes of compact sources of ≈30%, which includes additional uncertainties due to the fitting process needed to get integrated fluxes (Stickel et al. 2004). A second

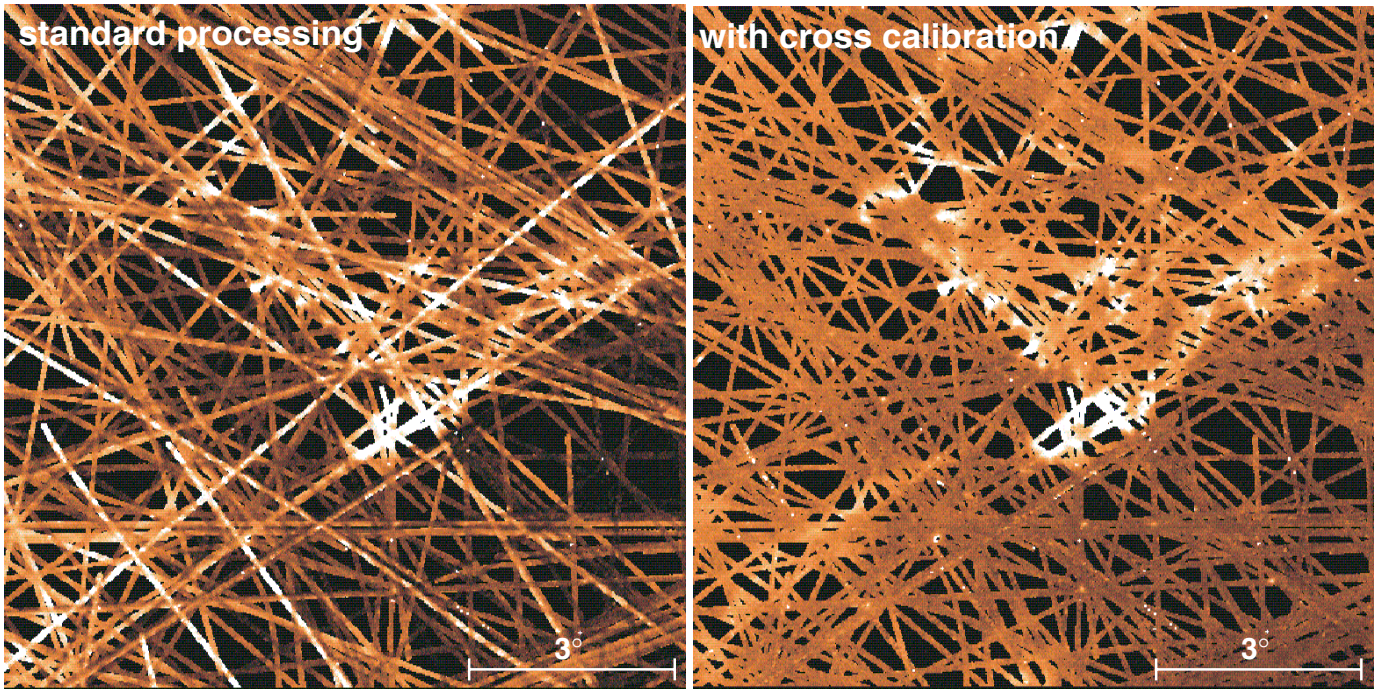

Fig. 3. A 10° × 10° region of the sky around the Draco cloud ($l \approx 90°$, $b \approx +38°$), an area with prominent galactic Cirrus structures at high galactic latitude. The map from the uncorrected slew data has a much larger scatter in brightness along individual slews (*left*) compared to the result after cross-calibration and rescaling (right). Surface brightnesses cover a range of 5–10 MJy/sr.

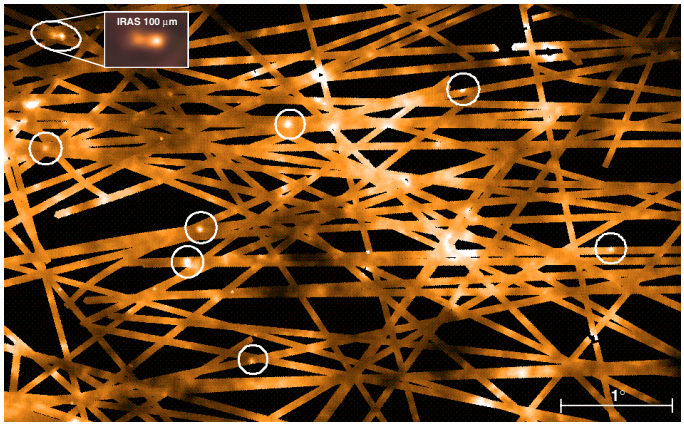

Fig. 4. An example of a map assembled from the rescaled ISOSS slew data. The image shows a typical sky region in the northern galactic hemisphere in Cygnus. Sources appearing in the ISOSS compact source database (Stickel et al. 2002, 2003) are encircled. The ellipse (*upper left*) indicates a close double source and the rectangular inset the corresponding region from the IRAS 100 μm survey, demonstrating the similar angular resolution. Surface brightnesses cover a range of 150–500 MJy/sr. The scale bar indicates 1°.

example (Fig. 4) demonstrates the high quality in angular resolution, matching quite well that of the IRAS 100 μm data, thereby alleviating the derivation of FIR color maps.

Ignoring a few outliers in each of the maps, which resulted from insufficiently corrected cosmic ray hits leaking into map pixels with almost no coverage from other slews, the overall dynamic range covers surface brightnesses of 1–1000 MJy/sr. The lower end is of the order of the integrated extragalactic background light and its absolute level is limited by the accuracy of the Zodiacal light subtraction. In a narrow strip directly in the galactic plane between $|b| \lesssim 2°$ and $|l| \lesssim 90°$, the data are saturated and can not be used. Coverage is densest around the North Ecliptic Pole ($l \approx 96°$, $b \approx 30°$), a region of low galactic cirrus contribution where an almost complete sky map could be obtained (Stickel et al. 1998a). For easy reference, Table 1 lists the galactic coordinates and the actual size of each map as well as the coverage of each map, so that individual objects of interest can be localized. The table columns denote the galactic longitude (Cols. 1, 6, 11) and latitude (Cols. 2, 7, 12), the size of each map in longitude (Cols. 3, 8, 13) and latitude (Cols. 4, 9, 14) and the sky coverage (Cols. 5, 10, 15). The final set of ISOSS Sky Atlas image files will be available from the ISO Data Archive and the CDS.

3. Initial scientific usage

3.1. Galaxies

The overall rescaling of the slew data has also been incorporated into the compact source database and the catalog of optically identified galaxies already contains the corrected 170 μm fluxes (Stickel et al. 2004). Furthermore, cross checking of the 170 μm fluxes for nearby galaxies resolved by the ISOPHOT Serendipity Survey has been done with the maps from the ISOSS Atlas plates. The coverage of the largest nearby spiral galaxy, M 31, is ≈50 (Fig. 5), and most of the major structures such as the ring morphology and the north-western knot can already be discerned. A detailed analysis of M 31 completely mapped at 170 μm can be found in Haas et al. (1998).

3.2. Medium and high mass star forming regions

A number of investigations of galactic star foming regions have already made use of the ISOSS Sky Atlas maps. Due to the longer wavelength observed, one can identifiy much colder

Table 1. The ISOPHOT Serendipity Survey Sky Atlas image list. The maps are arranged in galactic coordinates (l, b) and are presented in gnomonic projection. The coverage gives the percentage of the map area for which surface brightness information is provided. The coverage depends on the visibility of a certain sky area during the mission and the distribution of target pointings therein.

l [°] (1)	b [°] (2)	Δl [°] (3)	Δb [°] (4)	Coverage [%] (5)	l [°] (6)	b [°] (7	Δl [°] (8)	Δb [°] (9)	Coverage [%] (10)	l [°] (11)	b [°] (12	Δl [°] (13	Δb [°] (14)	Coverage [%] (15)
10	90	22	22	13.4	10	0	21	11	24.0	10	–55	23	22	13.1
10	75	22	22	17.4	30	0	21	11	25.9	40	–55	23	22	16.3
61.4	75	22	22	20.9	50	0	21	11	32.3	70	–55	23	22	21.5
112.8	75	22	22	16.5	70	0	21	11	40.6	100	–55	23	22	24.9
164.2	75	22	22	10.4	90	0	21	11	44.1	130	–55	23	22	23.4
215.7	75	22	22	6.4	110	0	21	11	46.5	160	–55	23	22	14.4
267.1	75	22	22	8.6	130	0	21	11	23.6	190	–55	23	22	9.4
318.5	75	22	22	14.8	150	0	21	11	13.7	220	–55	23	22	6.0
10	55	23	22	15.1	170	0	21	11	9.7	250	–55	23	22	11.4
40	55	23	22	23.9	190	0	21	11	5.3	280	–55	23	22	18.0
70	55	23	22	34.3	210	0	21	11	3.3	310	–55	23	22	15.5
100	55	23	22	32.1	230	0	21	11	1.4	340	–55	23	22	12.7
130	55	23	22	15.6	250	0	21	11	0.6	10	–75	22	22	12.3
160	55	23	22	6.8	270	0	21	11	1.6	61.4	–75	22	22	14.1
190	55	23	22	3.3	290	0	21	11	13.5	112.8	–75	22	22	14.4
220	55	23	22	5.0	310	0	21	11	23.5	164.2	–75	22	22	12.6
250	55	23	22	2.3	330	0	21	11	16.7	215.7	–75	22	22	13.3
280	55	23	22	4.7	350	0	21	11	18.7	267.1	–75	22	22	9.0
310	55	23	22	13.2	10	–15	21	20	12.3	318.5	–75	22	22	13.8
340	55	23	22	16.8	30	–15	21	20	19.0	10	–90	22	22	17.0
10	35	23	21	19.7	50	–15	21	20	18.7					
34	35	23	21	20.7	70	–15	21	20	16.7					
58	35	23	21	32.7	90	–15	21	20	23.0					
82	35	23	21	66.9	110	–15	21	20	25.7					
106	35	23	21	37.5	130	–15	21	20	20.3					
130	35	23	21	10.9	150	–15	21	20	15.7					
154	35	23	21	3.1	170	–15	21	20	19.1					
178	35	23	21	0.6	190	–15	21	20	14.5					
202	35	23	21	0.3	210	–15	21	20	10.6					
226	35	23	21	1.1	230	–15	21	20	6.5					
250	35	23	21	1.5	250	–15	21	20	4.6					
274	35	23	21	2.4	270	–15	21	20	3.9					
298	35	23	21	7.5	290	–15	21	20	14.3					
322	35	23	21	16.4	310	–15	21	20	15.4					
346	35	23	21	14.3	330	–15	21	20	10.6					
10	15	21	20	30.3	350	–15	21	20	12.3					
30	15	21	20	26.1	10	–35	23	21	16.6					
50	15	21	20	27.0	34	–35	23	21	18.9					
70	15	21	20	41.3	58	–35	23	21	14.8					
90	15	21	20	66.9	82	–35	23	21	18.1					
110	15	21	20	42.7	106	–35	23	21	21.2					
130	15	21	20	12.0	130	–35	23	21	21.0					
150	15	21	20	6.6	154	–35	23	21	12.4					
170	15	21	20	1.5	178	–35	23	21	9.4					
190	15	21	20	1.4	202	–35	23	21	9.6					
210	15	21	20	0.8	226	–35	23	21	10.5					
230	15	21	20	0.0	250	–35	23	21	14.4					
250	15	21	20	1.2	274	–35	23	21	23.7					
270	15	21	20	1.8	298	–35	23	21	18.5					
290	15	21	20	7.4	322	–35	23	21	12.2					
310	15	21	20	18.7	346	–35	23	21	12.3					
330	15	21	20	20.3										
350	15	21	20	27.7										

galactic sources, which are often younger and also more massive than those found with the IRAS survey data. A major effort has therefore been put on the detection and investigation of cold, massive and compact molecular clouds, promising candidates of massive star-forming regions at an early evolutionary stage.

The near-infrared (NIR) emission of already formed stars together with the strong FIR emission of a large dust mass still surrounding them is used to detect early stages of medium and high mass star forming regions. A subset of cold compact Serendipity Survey sources with 170 μm/100 μm flux ratio greater than 2 was

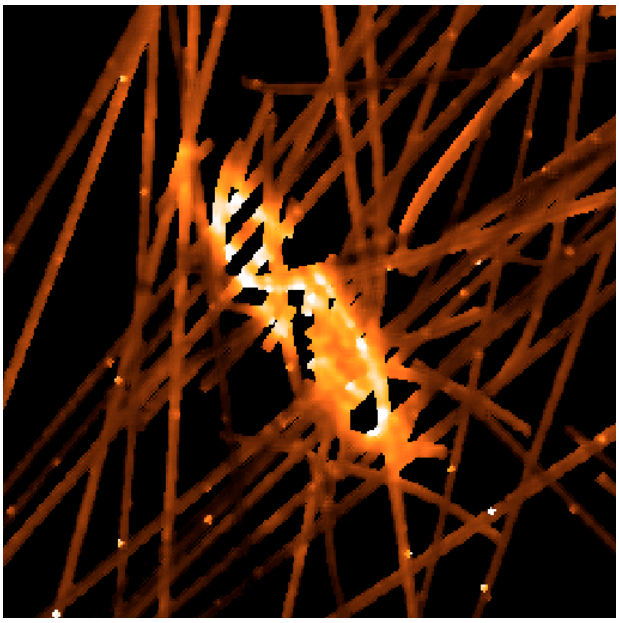

Fig. 5. Map of M 31 derived from all Serendipity Survey slews crossing the area. The large scale ring structure and the bright knot north-west of the center is apparent. (Cf. the fully sampled ISOPHOT 170 μm map by Haas et al. 1998.)

cross-correlated with source catalogues from the NIR 2MASS sky survey and the mid-IR MSX satellite mission. The high 170 μm/100 μm flux ratio indicates a large amount of cold dust, while the required NIR sources separate the sites with on-going star formation from cold interstellar cirrus structures. A large sample of ≈200 candidates has been collected, for which kinematic distances will be estimated from recent CO line emission (Krause et al. 2004a).

Sub-mm follow-up observations of three sources have already been obtained. Remarkably, the brightest sub-mm sources are in no case coincident with NIR sources, as expected for the less evolved objects in these regions. One of the investigated sources contains a young bright Herbig B2 star with ≈6 $M_\odot$ and estimated age of the less than 40 000 y, while in the adjacent region the dust is still very cold with a temperature of ≈12 K (Krause et al. 2003). The latest source investigated in detail is ISOSS J18364-0221 (Birkmann et al. 2006), which could be separated into two very cold and massive molecular cloud cores. One of them has a temperature and level of turbulence below the values found for massive cores so far, thus coming close to initial conditions from which high-mass star formation occurs. Follow-up investigations of these candidates for massive star-forming region is continuing with observations in the optical and NIR from the ground and NIR and MIR with Spitzer from space. It is planned to use the high angular resolution observations possible with the Herschel Space Observatory telescope in the FIR to eventually disentangle the different components in these regions and to determine profiles for the physical properties such as the dust temperature.

3.3. Cold galactic sources

The search for the coldest interstellar clouds and cloud cores within star-forming regions is based on the combination of the Serendipity Survey slew data with the surface brightnesses extracted from the IRAS/ISSA 100 μm and 60 μm maps. The IRAS data are smoothed to match the resolution of the Serendipity Survey slew data. The data are combined to give a two-dimensional color temperature map of the Galaxy, showing the distribution of the cold and warm regions on the sky (Fig. 6, Hotzel 2001). The largest clusters of cold cores with $T_{170/100} \approx 12$ K are found at galactic latitudes $|b| \approx \pm 15^\circ$ in the Taurus and Cepheus Flare regions, some in Chamaeleon and Ophiuchus, while Cygnus, Cepheus Main and Orion contain only warm cores. A comparison of the 170 μm/100 μm dust color temperature with the kinetic temperature of the gas in a sample of 14 ammonia cores showed a statistical correlation between the two temperatures (Hotzel 2001). This is remarkable, as it is not expected that gas and dust are directly thermally coupled.

The low temperatures for the coldest cores found are confirmed by high H_2 gas densities and low gas kinetic temperatures. Furthermore, the 170 μm surface brightness is correlated with optical extinction data over a much larger range than the 100 μm brightness, indicating that the 170 μm surface brightness is a very good tracer of dust column density. The initial study of the Chamaeleon region (Tóth et al. 2000) is being extended to cover the whole sky (Fig. 6), which will allow statistical studies of the cold cores and their correlation with other observational data. For the Taurus region, the generally low dust temperatures are confirmed by a detailed study of the Taurus Molecular Ring area with regular ISOPHOT imaging data (Tóth et al. 2004).

3.4. Late stages of stellar evolution

The large area coverage of the supernova remnant Cassiopeia A by the ISOSS 170 μm Sky Atlas was crucial to show that most of the sub-millimetre emission detected in this region is not associated with the remnant itself but originates from interstellar dust in a molecular cloud complex located in the line of sight to Cas A (Krause et al. 2004b). This invalided the earlier claim that a large amount of cold dust is present in the ejecta of this supernova remnant and that this particular object would support the general idea of supernovae being producers of copious amounts of dust. Follow-up observations of this region with Spitzer at 24 μm and from Calar Alto at 2 μm led to the discovery of moving structures with apparently high velocities outside the shell of the supernova remnant, interpreted as infrared echoes, in which interstellar dust is heated by the explosion and by flares from the compact object near the center of the remnant (Krause et al. 2005).

4. Concluding remarks

The large slew data base of the ISOPHOT Serendipity Survey has been assembled into the first large-scale sky atlas observed in the FIR at 170 μm. The most important scientific utilization makes use of supplementary IRAS 60 μm and 100 μm data for correlation and to uncover cold galactic sources of different astrophysical types. For the ongoing Japanese satellite mission AKARI (formerly ASTRO-F), the epoch observed by ISO between 1995 and 1998 provides a useful reference as its telescope is similar in size as ISO's and FIR confusion by cirrus due to limited angular resolution at the longest FIR wavelengths is similarly inescapable. Furthermore, for the up to now completely unexplored scientific area of variability of galactic and extra-galactic sources at FIR wavelengths on long time scales, only the Serendipity Survey data set can provide a significant increase in the covered time span.

Acknowledgements. We thank the referee, Tsutomu T. Takeuchi, for constructive and useful comments and suggestions, which improved the manuscript. The

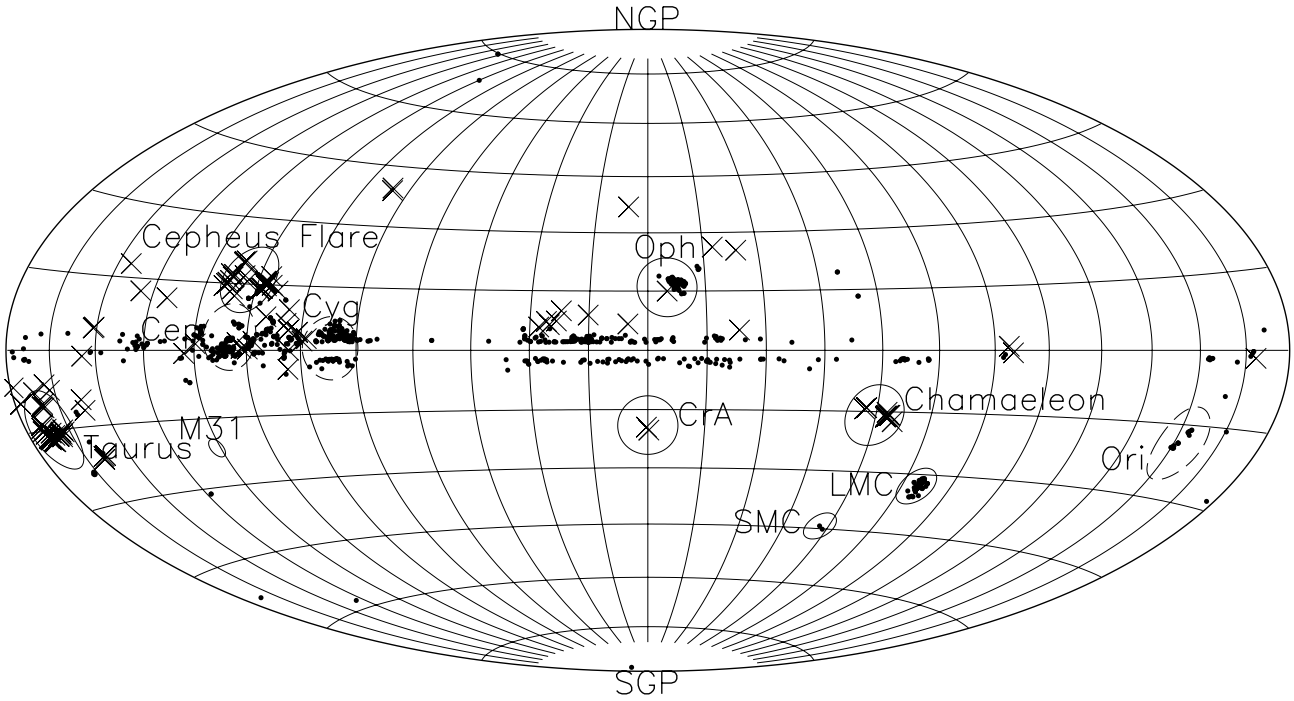

Fig. 6. The overall distribution of the coldest cores (crosses) with ISOSS 170 μm – IRAS 100 μm color temperatures below 12 K across the Milky Way. For comparison, warmer cores are indicated by filled dots. The largest cluster of very cold cores is found in the Taurus and Cepheus Flare region, both of which are associated with large molecular cloud complexes (Hotzel 2001).

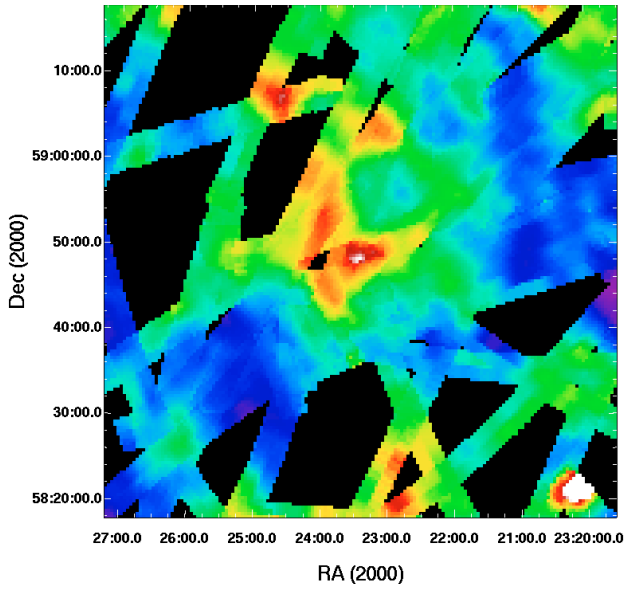

Fig. 7. Far-infrared emission from dust in the region of Cassiopeia A. The ISOPHOT 170 μm slew covers a $40' \times 80'$ field centered on Cas A. Colours represent the 170 μm surface brightness in the range 140–300 MJy/sr (Krause et al. 2004b).

development and operation of ISOPHOT were supported by MPIA and funds from Deutsches Zentrum für Luft- und Raumfahrt (DLR). The ISOPHOT Data Centre at MPIA is supported by Deutsches Zentrum für Luft- und Raumfahrt (DLR) with funds of Bundesministerium für Wirtschaft und Technologie, grant. No. 50 QI0201.

References

Birkmann, S. M., Krause, O., Lemke, D. 2006, ApJ 637, 380
Bogun, S. 1995, Dissertation, University of Heidelberg, Germany
Bogun, S., Lemke, D., Klaas, U., et al. 1996, A&A, 315, L71
Elvis, M., Plummer, D., Schachter, J., Fabbiano G. 1992, ApJS, 80, 257
Fruchter, A. S., & Hook, R. N. 2002, PASP 114, 144
Haas, M., Lemke, D., Stickel, M., et al. 1998, A&A, 338, L33
Hotzel, S. 2001, Dissertation, University of Heidelberg, Germany
Hotzel, S., Harju, J., Lemke, D., et al. 2001, A&A, 372, 302
Kessler, M. F. 1999, in The Universe as seen by ISO, ed. P. Cox, & M. F. Kessler, ESA SP 427, 23
Kessler, M. F., Steinz, J. A., Anderegg, M. E., et al. 1996, A&A, 315, L27
Krause, O. 2003, Dissertation, University of Heidelberg, Germany
Krause, O., Lemke, D., Tóth, L. V., et al. 2003, A&A, 398, 1007
Krause, O., Vavrek, R., Birkmann, S., et al. 2004a, Baltic Astron., 13, 407
Krause, O., Birkmann, S. M., Rieke, G. H., et al. 2004b, Nature 432, 596
Krause, O., Rieke, G. H., Birkmann, S. M., et al. 2005, Science, 308, 1604
Lemke, D., Burgdorf, M. 1992, in Infrared Astronomy with ISO (Nova Science Publishers, New York, Commack), ed. T. Encrenaz, & M. Kessler, 69
Lemke, D., Klaas, U., Abolins, J., et al. 1996, A&A, 315, L64
Müller, T. G., Hotzel, S., Stickel, M. 2002, A&A, 389, 665
Paige, C. C., & Saunders, M. A. 1982, ACM Trans. Math. Software 8, 43
Reach, W. T. 2000, SIRTF Background Estimation, Technical Report, IPAC, Pasadena
Reynolds, A. P., Parmar, A. N., Hakala, P. J., et al. 1999, A&AS, 134, 287
Sternberg, S. 1986, Computer Vision, Graphics and Image Processing 35, 333
Stickel, M., Bogun, S., Lemke, D., et al. 1998a, A&A, 336, 116
Stickel, M., Lemke, D., Bogun, S., et al. 1998b, ISOPHOT far-infrared serendipity sky survey, Proc. SPIE, 3349, 115
Stickel, M., Lemke, D., Bogun, S., et al. 1999, The ISOPHOT far-infrared serendipity sky survey, in The Universe as seen by ISO, ed. P. Cox, & M. F. Kessler, ESA SP 427, 839
Stickel, M., Lemke, D., Klaas, U., et al. 2000, A&A, 359, 865
Stickel, M., Lemke, D., Klaas, U., et al. 2002, Multi-Wavelength Data Mining of the ISOPHOT Serendipity Sky Survey, Proc. SPIE, 4847, 135
Stickel, M., Lemke, D., Klaas, U., Krause, O., et al. 2003, The Scientific Potential of the ISOPHOT 170 μm Serendipity Survey. in Exploiting the ISO Data Archive. Infrared Astronomy in the Internet Age, ed. C. Gry, et al., ESA SP-511, 169
Stickel, M., Lemke, D., Klaas, U., et al. 2004, A&A, 422, 39
Tóth, L. V., Hotzel, S., Krause, O., et al. 2000, A&A, 364, 769
Tóth, L. V., Kiss, C., Juvela, M., et al. 2002, A&A, 395, 663
Tóth, L. V., Haas, M., Lemke, D., et al. 2004, A&A, 420, 533